Maskless Photoassisted Micropatterning of Self-Assembled Monolayers through Thiol–Ene Click Chemistry

P. Covin, A. Airoudj, C. Minh Quoc Le, T. Buffeteau, P. Fioux, A. Spangenberg, F. Bally-Le Gall, C. Noël, T. Belmonte, V. Roucoules, et al.

Maskless photoassisted micropatterning of self-assembled monolayers through thiol-ene click chemistry

*P. Covin[1], A. Airoudj[1], C. Minh Quoc Le[1], T. Buffeteau[2], P. Fioux[1], A. Spangenberg[1], F. Bally-Le Gall[1], C. Noël[3], T. Belmonte[3], V. Roucoules[1], J. Carneiro de Oliveira[1]**

[1]Université de Haute-Alsace, Université de Strasbourg, CNRS, IS2M UMR 7361, 15 Rue Jean Starcky, 68100 Mulhouse, France

[2]Université de Bordeaux, ISM, UMR 5255 CNRS, 351 Cours de la Libération, 33405 Talence, France

[3]Université de Lorraine, CNRS, IJL, 2 allée André Guinier, BP 50840, F-54000 Nancy, France

Abstract

Reactive self-assembled monolayers are versatile interfaces that enable the design of chemical patterns with minimal topographical alteration. The development of efficient and fast strategies for generating such patterns is of relevance for the evolution of the field in terms of applications and of model substrates for fundamental studies. A strategy to functionalize reactive self-assembled monolayers is proposed in the present study. It takes advantage of photoinitiated thiol-

ene reaction to obtain chemical micropatterns via a maskless irradiation. The functionalization procedure occurred in only a minute and a detailed characterization of those surfaces allowed understanding their physico-chemical nature and the reactions involved. This study shows that by varying parameters such as photoinitiator molecule and wavelength of irradiation, effective modification of self-assembled monolayers can be achieved.

Introduction

The comprehension and control of interfacial phenomena often require the engineering of model surfaces. One common strategy for generating these surfaces is the use of self-assembled monolayers (SAMs). SAMs are the result of the ordered and spontaneous assembly of molecules into a one-molecule-thick layer on a solid surface[1]. They have been used in a wide range of applications, including sensors and biosensors[2,3], adhesion[4,5], biomolecules immobilisation[6–8], protective layers[9,10] and controlled growth of nanoparticles[11,12]. The broad scope of applications might conceal the relevance of the engineering process of SAMs and of all parameters that need to be considered. For instance, SAMs are substrate-selective. There is an intrinsic link between a molecule headgroup and its capability of self-organizing on a substrate as a monolayer. Thus, silane-based monolayers are commonly generated on silica oxide surfaces and thiol-based monolayers mostly on gold surfaces[13,14]. If a molecule attachment to a substrate is influenced by the headgroup, the ordering of the molecule into SAMs is affected by the spacers through van der Waals interactions with adjacent molecules. In addition, end-groups provide the final properties of a new interface created by the SAMs[1]. Those end-groups are therefore an important

component of self-assembled monolayers. Depending on to their nature, they can be used as a platform for further chemical reactions through functionalization.

The functionalization of the top groups of SAMs allows designing surfaces with varied chemical functionalities and controlled patterning. The functionalization presents the advantage of bringing chemical functions to the SAMs that would generally interfere in the self-assembly process if they were already present in the self-assembling molecule. In order to perform the functionalization, SAMs end-group should be reactive and vinyl-terminated monolayers have been largely used[15,16]. The functionalization of top groups can be achieved by a wide range of reactions[17]. Click chemistry reactions stand out as a relevant strategy for SAMs functionalization, given their commonly acknowledged efficiency and selectivity[18]. Some common click reactions include: azide–alkyne cycloaddition, Diels–Alder reaction and thiol-ene reaction[19]. The latter involves adding thiol molecules to alkenes to form thioethers. Previous studies used thiol-ene click chemistry to functionalize vinyl-terminated SAMs[20,21]. In particular, Campos *et al*. reported the possibility of achieving high yield of functionalization (45–75%) from a wide variety of functional thiols[20]. They tested a procedure using 2,2-dimethoxy-2-phenylacetophenone (DMPA) as photoinitiator and irradiation at 365 nm for 1.5 hours. Llevot *et al.* performed sequential reactions of α,ω-dithiols and α,ω-dienes with a vinyl-terminated SAMs using the same photoinitiator and irradiation wavelength for 2 hours[21].

One interesting aspect of SAMs functionalization is the possibility of creating chemical micropatterns. These patterns are of interest for many applications, such as controlled cell adhesion or microstructures growth[22,23]. Nevertheless, designing chemical micropatterns on self-assembled monolayers is challenging due to the complexity of the processes involved in their production. Micropatterns on SAMs are often tailored via soft lithography or

photolithography[1,17,20,21,24]. The former requires the elaboration of stamps and, commonly, handmade transfer of the pattern to the surface through methods such as microcontact printing. The latter is most often used in combination with soft lithography or via direct irradiation through a photomask. Thiol-ene click chemistry derived micropatterns have also been generated via a digital mirror device (DMD)[25], which can allow increase in throughput, and via beam pen lithography (BPL), which can improve miniaturization[26,27]. Localized ink deposition, such as microchannel cantilever spotting (μCS) and dip pen lithography (DPN), allowing to create mid- to high-resolution patterns have also been reported[28,29].

This work focuses on tailoring the functionalization and patterning of vinyl-terminated SAMs through thiol-ene chemistry. The use of self-assembled monolayers, and more specifically silane-based SAMs on native silicon oxide, enabled the formation of vinyl-terminated surfaces with homogeneous and defined chemistry. The functionalization by thiol-ene click chemistry was carried out with two thiols, resulting in surfaces terminated with either hydroxyl or carboxyl groups. SAMs functionalization was performed through a versatile maskless procedure with a photoinitiator and wavelength that, to the best of our knowledge, were not yet reported for thiol-ene functionalization of SAMs. The functionalization duration occurred within seconds. The selected approach aims to lift or reduce some technical and scientific barriers to the development and application of patterned SAMs, such as the use of photomasks or elastomeric stamps. All surfaces before and after functionalization were rigorously characterized and the possibility of limited side reactions of the photoinitiator with the SAMs was discussed. This provides evidence that not only the already acknowledge oxidation of thiol plays a role on side reactions on the surface[30]. The results obtained highlight the importance of combining the advances on methodologies of SAMs functionalization through thiol-ene reaction with detailed analysis of the

surface. The surfaces engineered through this strategy present potential applications in the control of nano-/microstructures formation and biomolecules immobilization, for instance.

Experimental Section

Preparation of vinyl-terminated self-assembled monolayer ($SiCH_2$)

Self-assembled monolayers were prepared using an adapted protocol from the literature[4,31]. Single- side polished silicon wafers (thickness of 380 µm, 1 × 1 cm^2; Silicon Material Inc.) were used as substrates. All wafers were successively rinsed with deionized water, ethanol and acetone. They were then dried and were placed in an ozone cleaner (UV/Ozone Cleaner; Bioforce Nanosciences®) for 30 minutes. The wafers were immersed in a 70% n- heptane (99%; Carlo Erba)/30% chloroform (99%; Carlo Erba) solution containing 1.0 mmol L^{-1} of 10-undecenyltrichlorosilane (95%; ABCR) and placed in a refrigerator at 4°C for 6 hours. The wafers were then successively rinsed with chloroform and deionized water at 80°C and dried under nitrogen flow. Finally, the samples were cleaned in an ultrasonic bath in chloroform for 15 minutes and dried under a nitrogen flow.

Functionalization by thiol-ene click chemistry

Functionalization was performed via thiol–ene chemistry after preparation of vinyl-terminated self-assembled ($SiCH_2$). 2-mercaptoethanol (≥99.0%; Sigma-Aldrich) enabled to obtain surfaces with a hydroxyl terminal group (SiOH) and 3-mercaptopropionic acid (≥99%; Sigma-Aldrich) allowed the preparation of surfaces terminated with a carboxylic acid group (SiCOOH). Functionalization was carried out using Ethylphenyl(2,4,6-trimethylbenzoyl)phosphinate (≥ 94.5%; Lambson Ltd UK), noted TPO-L, as photoinitiator. The vinyl surface was immersed in

thiol solution (typically, 20% vol. in N,N-Dimethylformamide DMF (99.9%; Carlo Erba), with 12.3 mg mL^{-1} TPO-L). For that, the sample is placed in a Petri dish (30 x 15 mm) and 2 mL of solution is then added to immerse the entire surface of the substrate. The Petri dish is then covered with a quartz lid to prevent evaporation of the solution. The system was then irradiated with a maskless lithography system (Smart Print UV; Microlight3D) under 385 nm UV equipped with a x1 objective lens (Model: Mitutoyo QV, N.A. 0.055) for 60 seconds (Irradiance: 4 mW/cm^2, measured at the sample level with a THORLABS PM100D equipped with S120VC photodiode power sensor) allowing photofunctionalization with sub-20 μm resolution. In order to irradiate the whole surface (1 x 1 cm^2), this step is replicated once to achieve a total irradiation time of 2 minutes. The surfaces were then rinsed with DMF and chloroform (99%; Carlo Erba) and dried under nitrogen flow. To remove any adsorbed compound, the samples were successively cleaned in an ultrasonic bath for 15 minutes in DMF followed by chloroform and dried under a nitrogen flow. The choice of 60 seconds of irradiation was decided through preliminary experiments that revealed no variation of contact angle values for higher irradiation times, up to 120 seconds.

Patterning

In order to create chemical patterns on the surface, the same procedure as for the functionalization was performed. The only difference was the spatially controlled irradiation of the samples. This spatial control was made possible by the maskless photolithography device (Smart Print UV; Microlight3D). A binary image (black and white) is projected onto the surface using Digital Micromirror Device (DMD) system. The DMD works by tilting microscopic mirrors to reflect light either towards or away from the sample. The white parts correspond to the

irradiated surface, while the black parts correspond to the non-irradiated surface. Two patterns were investigated. First, lines 16.5 µm wide (irradiated zone) were separated by 55.5 µm (non-irradiated zone). The second pattern was more complex and illustrated as a 60 µm long and 25 µm wide croissant. Binary images representative of these patterns are shown in Figure 1. Line patterns were obtained exactly through the functionalization procedure already described. Croissant patterns were obtained by using a x10 objective lens (Model: Mitutoyo QV, N.A. 0.28) for 6 seconds (Irradiance: 230 mW/cm^2, measured at the sample level with a THORLABS PM100D equipped with S120VC photodiode power sensor).

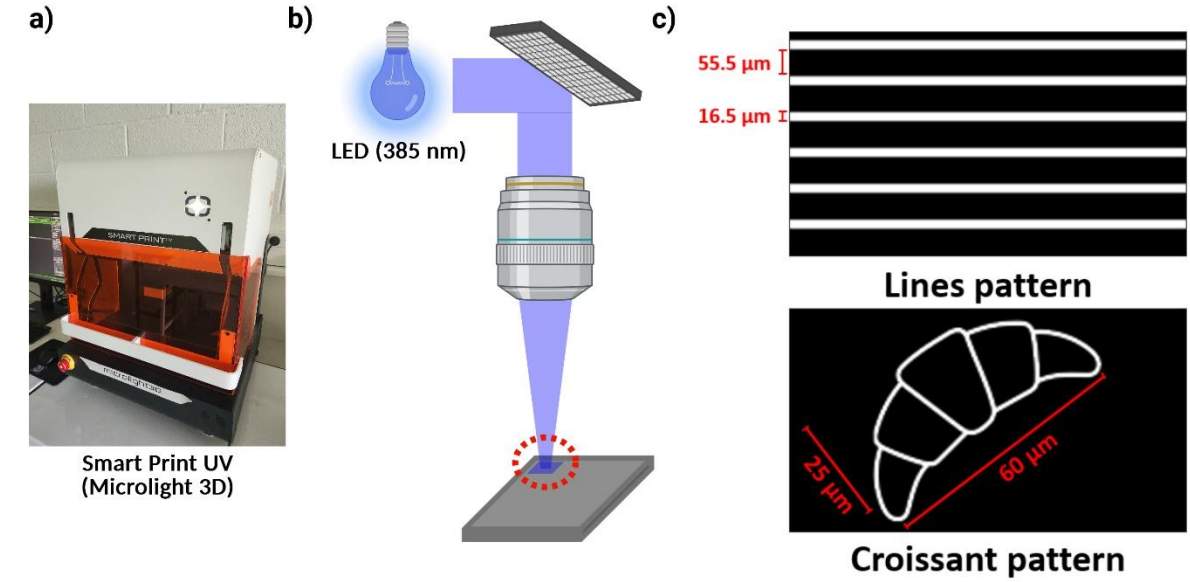

Figure 1. a) Photo of printer Smart Print UV (Microlight 3D) **b)** scheme of surface irradiation with the Digital Micromirror Device and **c)** binary image showing line patterns (top) and a croissant pattern (bottom). *Created in BioRender. kunemann, p. (2025) https://BioRender.com/5phj10y.*

Water contact angle measurements (WCA)

The static contact angles of deionized water were measured at room temperature (20°C) using a Drop Shape Analyzer (DSA100; Krüss). Droplets of 2 µL were carefully deposed on the surface using a syringe. Reported values are average of at least three water drops on three different samples. Contact angle hysteresis was also determined by measuring dynamic contact angles. To do this, a 4 µL water droplet was inflated at a rate of 1 $\mu L.s^{-1}$ for at least 10 s allowing the determination of the advancing angle. The volume of the inflated droplet was then reduced (at the same rate and over the same period) to measure the receding angle. The difference between the advancing and receding contact angles is the contact angle hysteresis.

Ellipsometry

The thicknesses of the SAMs were determined using a Jobin Yvon UVISEL (Horiba) with an incident angle of 70°. The Δ and ψ values were measured on each sample within a range from 1.5 to 6 eV in increments of 0.05 eV, with an integration time of 200 ms per increment. Data were fitted using the Cauchy model in DeltaPsi2 (v.2.6.8.239) software from the UVISEL ellipsometer.

Atomic force microscopy (AFM)

The surface morphology of the samples was analyzed using atomic force microscopy (AFM) in tapping mode under ambient conditions using a Flex AFM scanning probe microscope running with a Nanosurf C3000 controller (Nanosurf). Silicon cantilevers were used for all measurements (with ACT tip) with a spring constant of 13-77 Nm^{-1} and resonance frequency of 200-400 kHz, a width of 30 µm and a length of 125 µm. Lateral force microscopy (LFM) and

Kelvin probe force microscopy (KPFM) were carried out in a Bruker Multimode IV, with a Nanoscope V controller and an E "vertical" scanner.

For LFM, contact mode was used. All measurements were carried out using a ScanAsyst cantilever (Bruker) with a spring constant of 0.4 Nm^{-1} and resonance frequency of 70 kHz, a width of 25 μm and a length of 115 μm. KPFM used conductive AFM tips (EFM Pt/Ir-coating, NanoWorld) with a spring constant of 2.8 Nm^{-1} and resonance frequency of 75 kHz, a width of 28 μm and a length of 225 μm. Scanning was performed in lift mode based on a two-pass scan, including one trace and its retrace. During the first pass, a typical topological AFM image was captured in tapping mode with a zero tip bias on the trace and retrace. In the second pass, the AFM tip was lifted to 200 nm above the sample surface with an applied tip bias voltage. The sample was placed on a metal substrate using fast-drying silver paint and was set to electrical ground by connecting it to the sample bias control of the scanning probe microscope (SPM) controller. All the experiments were carried out in air and at room temperature. Data processing of multiscale images was performed using Gwyddion 2.65 software.

Polarization modulation infrared reflection absorption spectroscopy (PM-IRRAS)

For PM-IRRAS analysis, SiO_2/Au composite substrates were used. More precisely, the substrates were made of a silicon wafer coated with gold (100 nm) covered by SiO_2 layer of 205 Å (Si-Mat – Silicon Materials). This composite substrate allows the anchoring of a trichlorosilane and preserved the high reflectivity of gold for infrared radiation.

PM-IRRAS spectra were recorded on a ThermoNicolet Nexus 670 FTIR spectrometer at a resolution of 4 cm^{-1}, by coadding several blocks of 1500 scans (30 minutes acquisition time). Generally, ten blocks (5 hours acquisition time) were necessary to obtain PM-IRRAS spectra of

SAMs with good signal-to-noise ratios. Experiments were performed at an incidence angle of 75° using an external homemade goniometer reflection attachment[32]. The infrared parallel beam (modulated in intensity at frequency f_i lower than 5 KHz) was directed out of the spectrometer with an optional flipper mirror and made slightly convergent with a first BaF_2 lens (191 mm focal length). The IR beam passed through a BaF_2 wire grid polarizer (Specac) to select the p-polarized radiation and a ZnSe photoelastic modulator (PEM, Hinds Instruments, type III). The PEM modulated the polarization of the beam at a high fixed frequency, $2f_m$=100 KHz, between the parallel and perpendicular linear states. After reflection on the sample, the double modulated (in intensity and in polarization) infrared beam was focused with a second ZnSe lens (38.1 mm focal length) onto a photovoltaic MCT detector (Kolmar Technologies, Model KV104) cooled at 77 K. The polarization modulated signal I_{AC} was separated from the low frequency signal I_{DC} (f_i between 500 and 5000 Hz) with a 40 KHz high pass filter and then demodulated with a lock-in amplifier (Stanford Model SR 830). The output time constant was set to 1 ms. The two interferograms were high-pass and low-pass filtered (Stanford Model SR 650) and simultaneously sampled in the dual channel electronics of the spectrometer. In all experiments, the PEM was adjusted for a maximum efficiency at 2500 cm^{-1} to cover the mid-IR range in only one spectrum. For calibration measurements, a second linear polarizer (oriented parallel or perpendicular to the first preceding the PEM) was inserted between the sample and the second ZnSe lens. This procedure was used to calibrate and convert the PM-IRRAS signal in terms of the IRRAS signal (i.e. $1-\frac{R_p(d)}{R_p(0)}$, where $R_p(d)$ and $R_p(0)$ stand for the p-polarized reflectance of the film/substrate and bare substrate systems, respectively)[33,34].

X-ray photoelectron spectroscopy (XPS)

X-ray photoelectron spectroscopy (XPS) analyses were carried out using a VG SCIENTA SES-2002 spectrometer equipped with a concentric hemispherical analyzer. The incident radiation used was generated by a monochromatic Al Kα X-ray source (1486.6 eV) operating at 420 W (13 kV; 32.3 mA). Photoemitted electrons were collected at a take-off angle of 30° from the substrate surface, with electron detection in the constant analyzer energy mode (FAT). A wide scan spectrum signal was recorded with a pass energy of 500 eV, and for high-resolution spectra (S2s, O1s, Si2p, and C1s), the pass energy was set at 100 eV. The analyzed surface area was ~24 mm^2 and the vacuum pressure during XPS analysis was about 10^{-9} mbar. The spectrometer energy scale was calibrated using the Ag $3d^{5/2}$, $Au4f^{7/2}$, and $Cu2p^{3/2}$ core-level peaks, which were set at binding energies of 368.2, 84.0, and 932.6 eV, respectively. Spectra were subjected to a Shirley baseline and peak fitting was made with mixed Gaussian−Lorentzian components with equal full width at half-maximum (FWHM) using version 2.3.18 CasaXPS software (www.casaxps.com, Casa Software Ltd.). The surface composition expressed in atom % was determined by integrating peak areas of each component, taking into account the spectrometer's transmission factor, the mean free path, and the Scofield sensitivity factors of each atom (namely, C1s: 1; O1s: 2.93; Si2p: 0.95; and S2s: 1.43). All binding energies (BE) were referenced to the aliphatic C1s peak from the SAM or natural contamination at 285.0 eV with a step size of 0.1 eV.

The surface yield of the functionalization reactions were calculated from the wide scan spectra according to the formula:

$$Surface\ yield = \frac{Sulfur/Carbon}{Sulfur_{theo.}/Carbon_{theo.}} \quad (1)$$

where Sulfur and Carbon are the atomic percentages of sulfur and carbon determined on the XPS wide scan and $Sulfur_{theo.}$ and $Carbon_{theo.}$ are the atomic percentages of sulfur and carbon calculated from the grafted chain (SAMs + thiol).

Results and Discussion

SAMs Characterization and Functionalization

A detailed analysis of vinyl-terminated SAMs ($SiCH_2$) before and after functionalization with carboxylic acid or hydroxyl end group (SiCOOH and SiOH, respectively) was performed. The goal was firstly to characterize as accurately as possible the original vinyl-terminated monolayer, and secondly, to understand the functionalization process and assess any possible side reactions prior to patterning. To better visualize the chemical modifications, the structures of the $SiCH_2$, SiOH, and SiCOOH surfaces are shown in Figure 2.

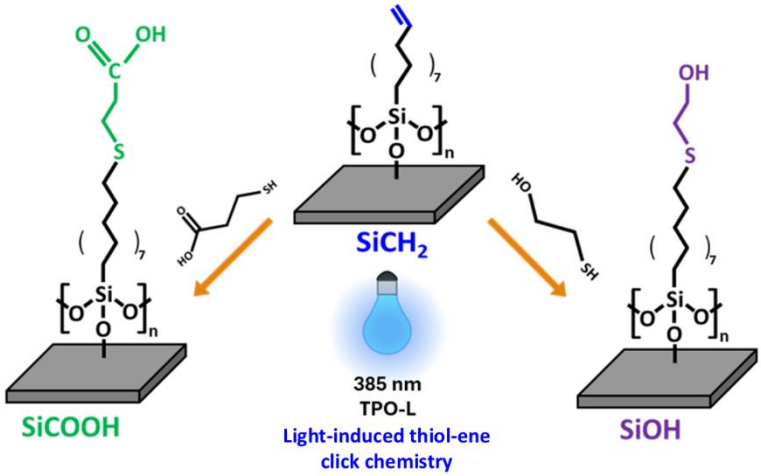

Figure 2. Schematic illustration of the surface functionalization process: A vinyl-terminated SAM is post-functionalized by thiol-ene click chemistry with TPO-L (photoinitiator) and UV light (385 nm).

Water contact angle

Vinyl-terminated SAMs ($SiCH_2$) had static water contact angles of 100 ± 2° (Table 1). This value is consistent with a well-defined and ordered self-assembled monolayers derived from 10-undecenyltrichlorosilane[15]. Additionally, the water contact angle hysteresis was 11° which is consistent with the expected behavior of well-organized vinyl-terminated monolayers[35]. Hydroxyl (SiOH) and carboxyl-terminated monolayers (SiCOOH) had static water contact angles of 56 ± 4° and 46 ± 2°. Compared with the vinyl-terminated surface, there was a significant reduction in the contact angle, from 100° to almost 50°, regardless of the thiol used. Macroscopically, this decrease shows a change in surface chemistry from hydrophobic to hydrophilic, consistent with the expected surface functionalization[20]. The increase in water contact angle hysteresis (Table 1) is a result of the change in surface hydrophilicity. These results enable an initial assessment of the quality of the prepared SAMs and its thiol-ene functionalization. Nevertheless, it is not possible to distinguish between the chemistry and morphology of the surface, so complementary analysis were performed in this regard.

Table 1. Water static contact angles and water contact angle hysteresis values of the vinyl-terminated ($SiCH_2$), hydroxyl-terminated (SiOH) and carboxyl-terminated (SiCOOH) SAMs.

SAMs	Water static contact angles (°)	Water contact angle hysteresis (°)
$SiCH_2$	100 ± 2	11 ± 4
SiOH	56 ± 4	20 ± 4
SiCOOH	46 ± 2	21 ± 4

Ellipsometry

The experimental thickness of around 15 Å for $SiCH_2$ SAMs is consistent with a monolayer prepared from 10-undecenyltrichlorosilane (Table 2)[15]. The comparison of that measured thickness value with a theoretical value is mostly consistent[36]. The difference of around 2 Å between theoretical and measured value is probably due to the formula used, which consider methyl-terminated SAMs and chains in an all-*trans* conformation[36].

Table 2. Measured, calculated and literature thickness values of $SiCH_2$, SiOH and SiCOOH SAMs

SAMs	Measured thickness (Å)	Calculated thickness (Å)	Literature values (Å)
$SiCH_2$	15 ± 1	17[36]	15 ± 2[15]
SiOH	21 ± 3	21[36]	-
SiCOOH	21 ± 3	21[36]	-

Table 2 also presents the thickness values of the hydroxyl and carboxyl-functionalized monolayers. The experimental values determined by ellipsometry are close to the theoretical calculated thickness for both functionalized surfaces. These thickness results are consistent with the expected outcome of thiol-ene functionalization of the SAMs.

Atomic force microscopy (AFM)

To further assess the quality of the SAMs, AFM was used as complementary to the thickness analysis. Typical AFM topography result of the vinyl-terminated SAM ($SiCH_2$) is shown in Figure 3. The image shows smooth and flat surfaces with root mean square roughness (RMS)

values of 0.2 nm averaged over an area of 10×10 μm^2. RMS values lower than 0.3 nm, are distinctive of well-defined monolayers[17]. Figure 3 also shows typical AFM results for the hydroxyl (SiOH) and carboxyl-functionalized monolayers (SiCOOH). The two images show mainly smooth and flat surfaces with RMS values of 0.3 nm. The AFM results indicate that the functionalization protocol used does not produce any significant change in surface morphology hinting to the efficient chemical reaction between the self-assembled monolayer and the thiols.

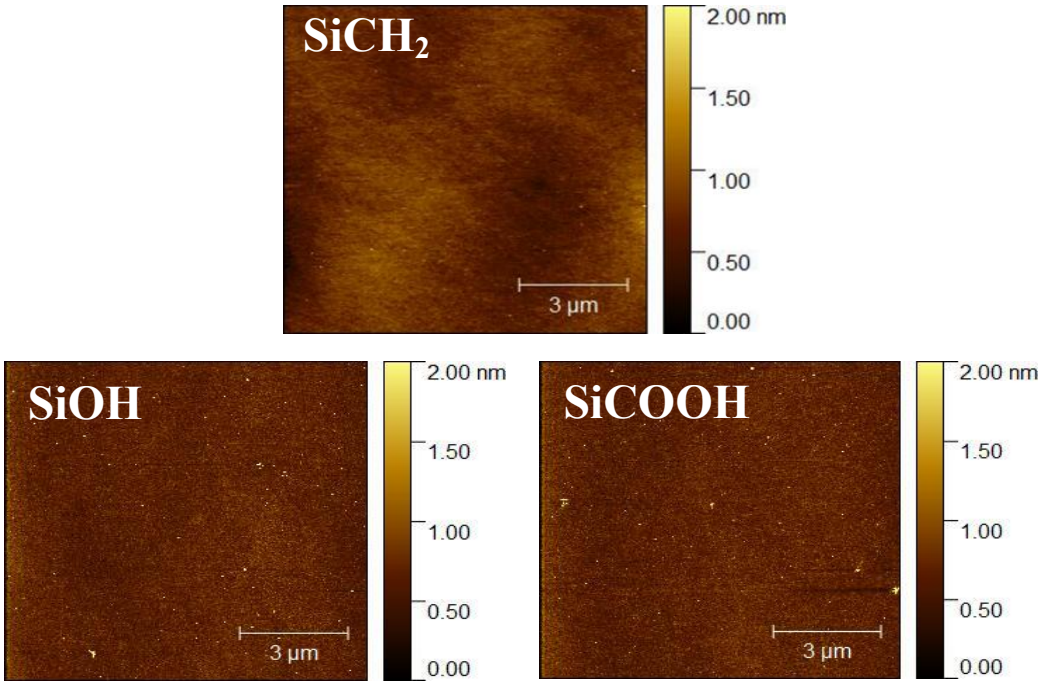

Figure 3. Height AFM images (10 x 10 μm^2) of vinyl-terminated SAMs ($SiCH_2$), hydroxyl-terminated monolayers (SiOH) and carboxyl-terminated monolayers (SiCOOH).

The combined AFM, ellipsometry and contact angle analyses provide strong evidence of the formation and functionalization of smooth and homogenous SAMs. However, the contact angle and AFM results only evidence that chemical changes after functionalization occur without morphological variation. They do not allow to conclusions to be drawn about the chemical bonds

and reactions that are actually taking place. These results are thus complemented by spectroscopic analysis.

X-ray photoelectron spectroscopy (XPS)

Figure 4 shows the XPS wide scan and high-resolution spectra of C1s for the vinyl-terminated SAMs. As expected, XPS wide scan showed the presence of Si (2p at 99.5 eV), C (1s at 285.0 eV) and O (1s at 532.5 eV). The spectra distinguish between the bulk Si (Si 2s at 150.8 eV, Si 2p at 99.2 eV), and the silicon oxide (Si 2s at 154 eV, Si 2p at 103.2 eV). The chemical composition was consistent with that of non-contaminated films. There were no unexpected elements detectable in the films, nor any sign of unreacted material, such as a Cl peak.

In the high-resolution spectrum, it is not possible to distinguish between single and double carbon bonds (285 eV). In fact, the energy difference between the methyl and the vinyl C1s signal is lower than the XPS resolution (~0.4 eV), and the signal for the single C=C bond should be weak due to a single double bond per molecule[15]. There is a possibility of small amounts (around 3%) of C-O contamination (286.5 eV). The signal from such species would also contribute to the aliphatic carbon peak. These results are consisted to those reported in the literature in terms of atomic percentage and amount of contamination[15].

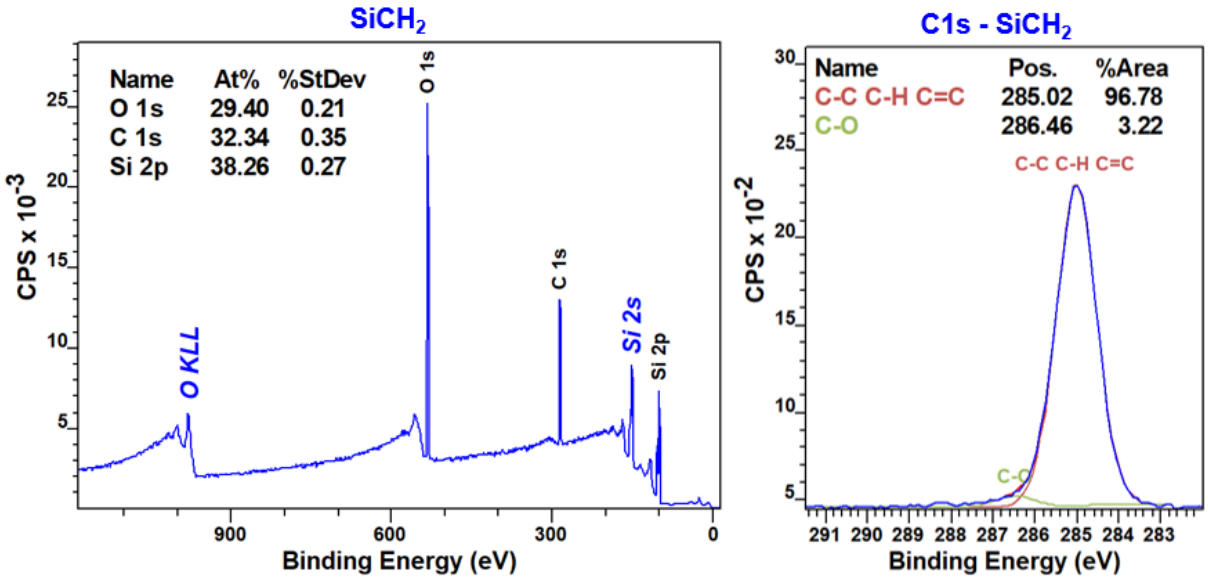

Figure 4. XPS wide scan spectra of vinyl-terminated SAMs (left) and XPS C1s high-resolution spectra of vinyl-terminated SAMs (right).

XPS analyses were also carried out on the samples functionalized with each thiol. Figure 5 shows the wide scan and high-resolution XPS spectra of C1s for hydroxyl (SiOH) and carboxyl-functionalized monolayers (SiCOOH).

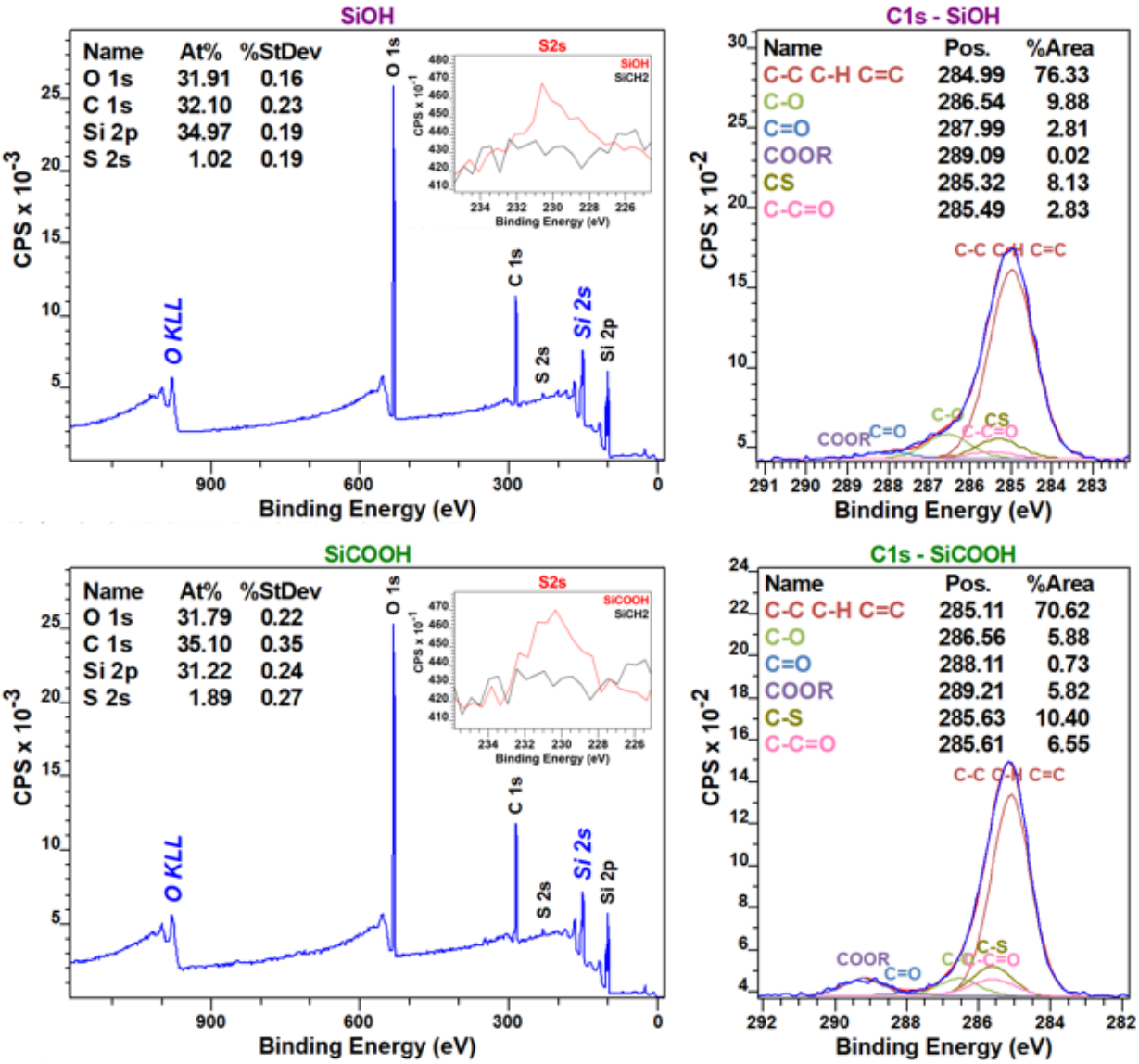

Figure 5. XPS wide scan and C1s high-resolution spectra of hydroxyl-terminated monolayers (SiOH) and carboxyl-terminated monolayers (SiCOOH) photoinitiated by TPO-L *Inset: focus on the S2s region and comparison between the $SiCH_2$ (black) and SiOH or SiCOOH (red).*

As expected, the XPS wide scans for both functionalized surfaces show the presence of Si (2p at 99.5 eV), C (1s at 285.0 eV), O (1s at 532.5 eV) and S (2s at 231 eV). The presence of S2s in

the wide-scan spectrum highlights the functionalization of the vinyl-terminated monolayer by thiol-ene click chemistry for both thiols.

Surface yield values, obtained by the S/C ratios as described in the experimental part, of 43 ± 3 % for SiOH and 83 ± 7 % for SiCOOH were obtained. These results fall in the range of what is reported by other authors for different functionalization conditions involving different thiols, wavelength and photoinitiator used[20].

By comparing the high-resolution C1s spectrum before and after functionalization for the hydroxyl functionalization, an increase in the C-O component is clearly observable. This increase can be explained by the addition of terminal hydroxyl functions, which is consistent with the expected functionalization reaction. The spectrum shows components corresponding to carbonyl and carboxyl groups (C=O; COOR), suggesting a small contamination (around 3%) or oxidation of the contamination already present on the $SiCH_2$. Together with the appearance of the sulfur and the analysis of C1s spectrum, a decrease in the amount of Si2p after functionalization has been used to indicate the thiol-ene click chemistry[21]. Those features are observed in this study.

Comparing the high-resolution C1s spectrum before and after functionalization for the SiCOOH sample clearly shows the appearance of a COOR component. This increase can be explained by the addition of terminal carboxyl functions, which is consistent with the expected functionalization reaction. The spectrum shows components corresponding to carbonyl groups (C=O) and C-O groups – around 7%. One possible explanation for the presence of these groups is contamination of the monolayer, which can occur given the high sensitivity and reactivity of the surface carboxyl groups. Another hypothesis is the presence of side reactions during functionalization, leading to a certain proportion of carbonyl and C-O functions. A control

experiment has revealed that the second hypothesis is indeed correct and that the side reactions take place between the photoinitiator (TPO-L) and the $SiCH_2$ surface (Figure 6). Figure 6 shows the XPS of a reference surface exposed to the same conditions used for functionalization, in the presence of TPO-L but in the absence of thiol. It indicates that the photoinitiator undergoes secondary reactions with the surface. The C1s high-resolution spectrum shows a slight increase in C-O, already present on $SiCH_2$ as contamination, and the appearance of C=O and a very small amount of COOR components. The results indicate that TPO-L play a role in the oxidation of SAMs, beyond being merely an initiator for the thiol-ene reaction. These same secondary reactions might be responsible for the unexpected components observed in the reactions with each thiol. Nevertheless, their XPS spectra reveal that thiol reaction with the surface remains the main reaction taking place. Further control experiments such as irradiating the SAMs only in the presence of the thiol in DMF or the SAMs only in DMF gave similar contact angle results (96° ± 2°), indicating that thiol-ene grafting reaction in the tested conditions are quite dependent of the presence of the photoinitiator.

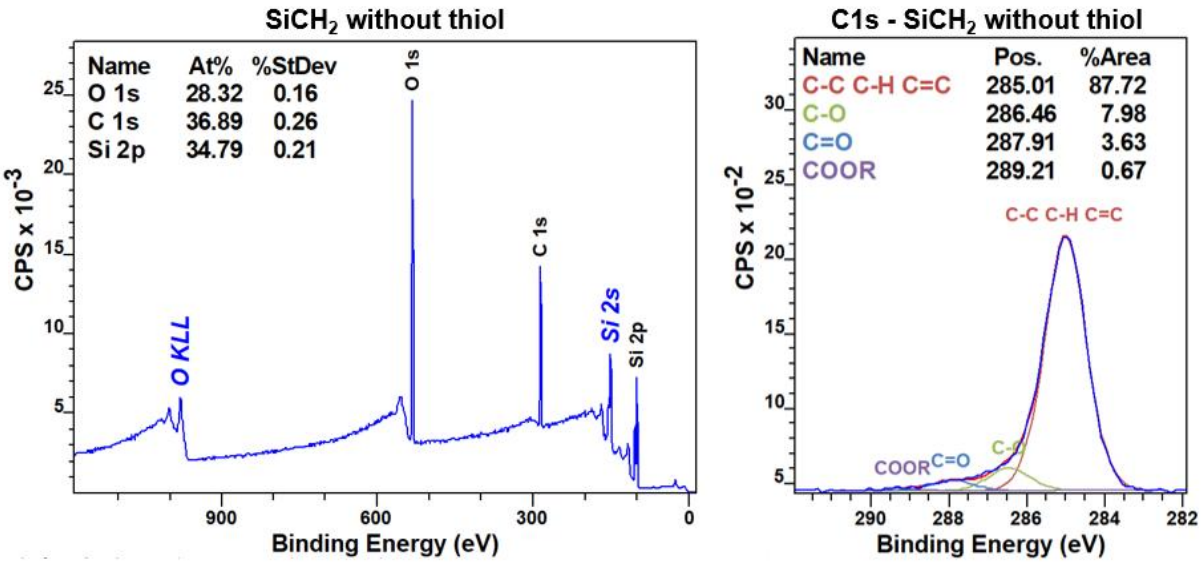

Figure 6. XPS wide scan and C1s high-resolution spectra of irradiated vinyl-terminated monolayers (SiOH) in DMF and with TPO-L (photoinitiator).

Polarization modulation infrared reflection absorption spectroscopy (PM-IRRAS)

Figure 7 shows the experimental PM-IRRAS spectra of the substrate functionalized with a vinyl-terminated SAMs ($SiCH_2$). In this spectrum, the bands associated with different functional groups of the monolayer are clearly visible. The following characteristic vibrational bands were identified: asymmetric (ν_aCH_2) and symmetric (ν_sCH_2) stretching modes of methylene groups at 2927 cm^{-1} and 2855 cm^{-1}, respectively, and the bending mode (δCH_2) around 1465 cm^{-1} related to the alkyl chains. The bands located at 3082 and 3002 cm^{-1} are assigned to the νCH stretching modes of CH_2 and CH of terminal vinyl groups, respectively, which is consistent with the expected results. Based on the work of Snyder et al.[37] wavenumbers observed in Figure 7 for the ν_aCH_2 (2927 cm^{-1}) and ν_sCH_2 (2855 cm^{-1}) bands indicate the presence of a large number of *gauche* conformations in the alkyl chains of the grafted molecules.

The infrared spectra of hydroxyl- and carboxyl-functionalized monolayers obtained by PM-IRRAS are shown in Figure 7. Regarding SiOH surface, the vibrational bands related to the methylene groups of the alkyl chains (ca ν_aCH_2, ν_sCH_2 and δCH_2) were observed at the same wavenumbers with slightly higher intensities than those measured for vinyl-terminated SAM. The bands located at 3082 and 3002 cm^{-1}, related to the νCH stretching modes of CH_2 and CH of terminal vinyl groups, respectively, disappeared and new bands around 3345 and 1380 cm^{-1} appeared. The broad band around 3345 cm^{-1} is related to the stretching νOH mode, whereas the band located at 1380 cm^{-1} is assigned to the bending δCOH mode of the hydroxyl-terminated groups. Thus, the bands associated with hydroxyl functional groups are clearly visible as well as the carbon chains grafted onto the substrate, which is in accordance with a successful functionalization of the vinyl-terminated SAM.

Regarding the spectrum of the SiCOOH surface, the bands corresponding to the carboxyl functional groups and the alkyl chains can be assigned. The vibrational bands related to the methylene groups of the alkyl chains (ca ν_aCH_2, ν_sCH_2 and δCH_2) were observed at the same wavenumbers with similar intensities than those measured for hydroxyl-terminated SAM. In addition, it is possible to identify two bands at 1730 and 1675 cm^{-1} that can be attributed to the carbonyl stretching vibration (νC=O) of carboxylic acid groups, free (1730 cm^{-1}) or involved in hydrogen bonding (1675 cm^{-1}). Finally, the band located at 1384 cm^{-1} is assigned to the bending δCOH mode of the carboxyl-terminated groups.

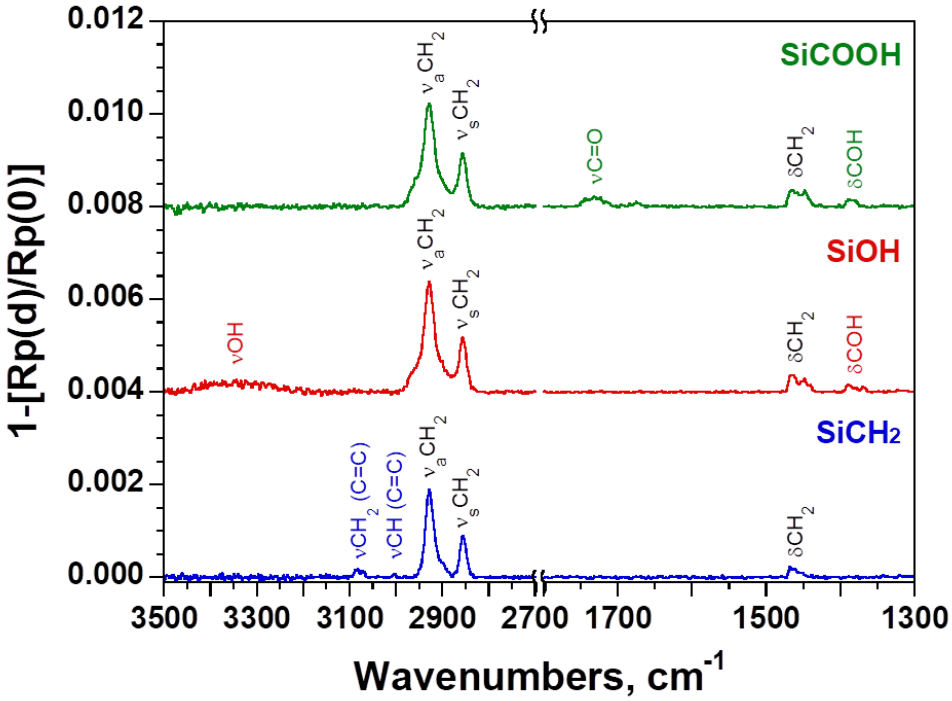

Figure 7. PM-IRRAS spectra of vinyl-terminated SAMs ($SiCH_2$), hydroxyl-terminated monolayers (SiOH) and carboxyl-terminated monolayers (SiCOOH).

The presence of the functional groups from the thiol compound is clearly visible for each thiol on the functionalized SAMs, which constitutes an unwavering proof of successful thiol-ene reactions. Furthermore, after functionalization, it is possible to highlight the disappearance of the bands corresponding to the νCH stretching modes of CH_2 and CH of terminal vinyl groups. The disappearance of the vinyl group associated with the appearance of the COH and COOH groups for each thiol is consistent with the occurrence of the expected thiol-ene click reactions.

Throughout this section, we have validated a procedure for the preparation of vinyl-terminated SAMs and, most importantly, we have elaborated a strategy for their functionalization with TPO-L as a photoinitiator and UV-light at 385 nm. The results presented so far clearly indicate that densely packed, smooth, and homogeneous monolayers were generated for the trichlorosilane used. For both functionalized surfaces, all the performed analyses indicated a successful

functionalization of the prepared SAMs with either hydroxyl- and carboxyl-terminated thiols. A small amount of side reactions was also evidenced. Although small amounts of side reaction could be observed, the surface yield calculated by XPS confirmed that they remained limited compared to the thiol-ene reaction. To generate chemical contrast on a single surface, we tested the spatial control of the reaction through the same maskless procedure in order to design chemical patterns on the SAMs.

Micropatterned surfaces

Here light irradiation is explored as a way to spatially control the thiol-ene reaction, enabling the creation of micropatterns with different chemistries (Figure 1). To highlight the presence of this micrometric chemical contrast, the samples were analyzed using two AFM modes: Lateral Force Microscopy (LFM) and Kelvin Probe Force Microscopy (KPFM). LFM consists of measuring the lateral friction forces between the tip and the sample, which are obtained from the torsion of the cantilever. In the KPFM mode, local surface potential is measured by detecting electrostatic forces between the tip and the sample, typically using a two-pass technique (lift) to separate topography and potential signals.

Both the LFM friction and KPFM potential images clearly identify contrast between the irradiated and the non-irradiated areas of the sample, with each area corresponding to distinct chemistry ($SiCH_2$/SiCOOH or $SiCH_2$/SiOH) (Figure 8). Regarding the LFM results, the dark areas can be attributed to vinyl-terminated areas (low friction), while the bright areas correspond to hydroxyl- and carboxyl-terminated areas (high friction)[38]. When comparing the contrast obtained using different thiols (hydroxyl- or carboxyl-terminated), the contrast is lower for patterns made with the hydroxyl-terminated thiol. This observation can be explained by the

chemistry itself. Indeed, it has been observed that the relative lateral force between methyl and hydroxyl groups is weaker than with carboxyl groups[38]. Similar behavior can be expected for the contrast with vinyl groups. The lower surface yield for the hydroxyl surface, observed in XPS, also justifies this difference. In KPFM measurements, the difference in surface potential between carboxyl/hydroxyl areas to vinyl areas is consistent with the literature on similar surfaces[39–42].

Compared with the theoretical size of the lines (16.5 μm), it is possible to observe a broadening whatever the thiol and the techniques (LFM or KPFM) used. Indeed, for carboxyl-terminated thiol, the broadening is around 3 μm (18 ± 2 μm lines) in KPFM and 5 μm (20 ± 3 μm lines) in LFM. For hydroxyl-terminated thiol, the broadening is of around 9 μm (20 ± 4 μm) in KPFM and of 14 μm (30 ± 5 μm) in LFM. The differences in size between the designed pattern and the real one are due to the resolution of each technique, focus adjustment during the irradiation process and the probable diffusion of the light and reactive species during this process.

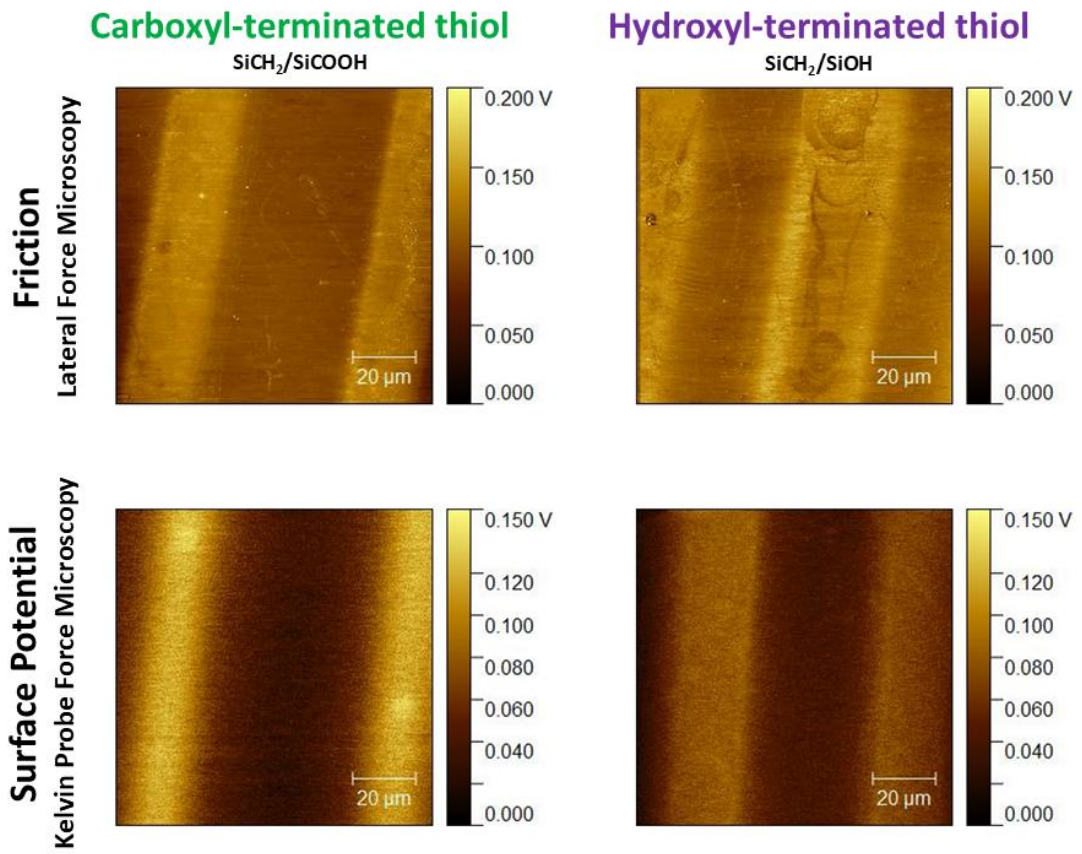

Figure 8. Lateral Force Microscopy friction (100 × 100 µm^2, top) and Kelvin Probe Force Microscopy potential (100 × 100 µm^2, bottom) images of line-patterned vinyl-terminated SAMs ($SiCH_2$) by light-induced thiol-ene click chemistry using carboxyl-terminated thiol (left) and hydroxyl-terminated thiol (right).

In terms of technique, KPFM consistently produces greater contrast in image between functionalized and non-functionalized zones than LFM does, for both thiols used. This difference can be explained by the sensitivity of the technique and its acquisition method. Indeed, unlike friction measurement, which requires contact with the surface, surface potential measurement is carried out at a distance from the sample (lift mode). Consequently, the surface potential images obtained are not disturbed by small surface heterogeneities. The result is a cleaner image for KPFM.

To demonstrate that SAMs functionalization can also be achieved for more complex patterns, a croissant pattern was used. Topography and potential image obtained in KPFM for croissant-patterned vinyl-terminated SAMs ($SiCH_2$) by thiol-ene click chemistry using carboxyl-terminated thiol is shown in Figure 9.

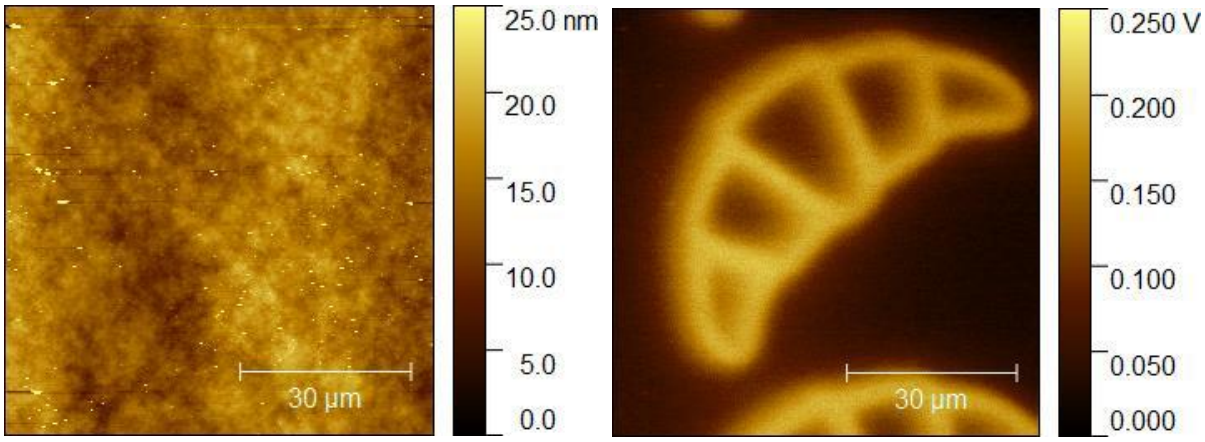

Figure 9. Atomic force microscopy height image (70 x 70 μm^2, left) and Kelvin Probe Force Microscopy potential image (70 × 70 μm^2, right) of croissant-patterned vinyl-terminated SAMs ($SiCH_2$) by light-induced thiol-ene click chemistry using carboxyl-terminated thiol.

As with the line patterns, the croissant pattern can be observed by surface potential contrast with no distinctive morphological changes in topography (Figure 9). The bright areas correspond to carboxyl-terminated surface chemistry (SiCOOH), while the dark areas correspond to vinyl-terminated surface chemistry ($SiCH_2$). Comparing the theoretical size of the pattern (60 µm long, 25 µm wide) with the one obtained (64 µm long, 28 µm wide), a broadening of approximately 3 µm is observed. This is comparable to the broadening measured in the case of lines (in Figure 8 for SiCOOH using KPFM) and can be explained in the same way. This result shows that, through the procedure developed in this work, it is possible to obtain controlled interfaces with relatively complex chemical patterns and without morphological features through a straightforward approach.

Conclusion

Densely packed, smooth, and homogeneous monolayer were generated from 10-undecenyltrichlorosilane. The analyses presented in this study revealed a successful functionalization of the prepared SAMs with a hydroxyl and carboxyl-terminated thiol. This study evidenced the importance of carefully characterizing SAMs to assess their quality and functionalization. The possibility of limited side reactions between TPO-L and vinyl-terminated SAMs during functionalization was also discussed. The detailed analysis of surfaces performed in this work enabled us to conclude about the limitation of those side reactions when compared to the targeted thiol-ene. For many applications, we consider that the most relevant result is the ability to generate a well-defined chemical contrast rather than a flawless functionalization procedure, hardly achievable by thiol-ene chemistry. In addition, we propose that XPS combined with PM-IRRAS are important tools for analyzing SAMs and for making a critical decision on the pertinence of a functionalization procedure for a specific application. Chemical micropatterns on vinyl-terminated SAMs were obtained through a simple, straightforward and fast procedure, after only 60 seconds of irradiation with a maskless device.

Corresponding Author

* J. Carneiro de Oliveira – Email: jamerson.carneiro-de-oliveira@uha.fr

Author Contributions

The manuscript was written through contributions of all authors. All authors have given approval to the final version of the manuscript.

Acknowledgment

The authors acknowledge the ANR – FRANCE (French National Research Agency) for its financial support of the project SPON-TO-CTRL (ANR-22-CE51-0018). This work was supported by a French government grant managed by ANR under the France 2030 program (Project Mat-Light 4.0 - ANR-21-EXES-0012).

References

(1) Nicosia, C.; Huskens, J. Reactive Self-Assembled Monolayers: From Surface Functionalization to Gradient Formation. *Mater. Horiz.* **2013**, *1* (1), 32–45. https://doi.org/10.1039/C3MH00046J.

(2) Singh, M.; Kaur, N.; Comini, E. The Role of Self-Assembled Monolayers in Electronic Devices. *J. Mater. Chem. C* **2020**, *8* (12), 3938–3955. https://doi.org/10.1039/D0TC00388C.

(3) Hayashi, T.; Latag, G. V. Self-Assembled Monolayers as Platforms for Nanobiotechnology and Biointerface Research: Fabrication, Analysis, Mechanisms, and Design. *ACS Appl. Nano Mater.* **2025**, *8* (17), 8570–8587. https://doi.org/10.1021/acsanm.5c00790.

(4) Tomasovic, L.; Fioux, P.; Gilbert, F.; Jacquet, D.; Verchère, D.; Bally-Le Gall, F.; Ponche, A. Self-Assembled Monolayers with a Controlled Density of Hydroxyl Groups: A Relevant Model to Investigate the Adhesion Properties of Epoxy Adhesives. *J. Phys. Chem. C* **2022**, *126* (6), 3227–3234. https://doi.org/10.1021/acs.jpcc.1c10432.

(5) Chin, L. C.; Ang, X. F.; Wei, J.; Chen, Z.; Wong, C. C. Enhancing Direct Metal Bonding with Self-Assembled Monolayers. *Thin Solid Films* **2006**, *504* (1–2), 367–370. https://doi.org/10.1016/j.tsf.2005.09.070.

(6) Wadu-Mesthrige, K.; Amro, N. A.; Liu, G.-Y. Immobilization of Proteins on Self-Assembled Monolayers. *Scanning* **2000**, *22* (6), 380–388. https://doi.org/10.1002/sca.4950220607.

(7) Prime, K. L.; Whitesides, G. M. Self-Assembled Organic Monolayers: Model Systems for Studying Adsorption of Proteins at Aurfaces. *Science* **1991**, *252* (5009), 1164–1167. https://doi.org/10.1126/science.252.5009.1164.

(8) Jonkheijm, P.; Weinrich, D.; Schröder, H.; Niemeyer, C. M.; Waldmann, H. Chemical Strategies for Generating Protein Biochips. *Angewandte Chemie International Edition* **2008**, *47* (50), 9618–9647. https://doi.org/10.1002/anie.200801711.

(9) Hutt, D. A.; Liu, C. Oxidation Protection of Copper Surfaces Using Self-Assembled Monolayers of Octadecanethiol. *Applied Surface Science* **2005**, *252* (2), 400–411. https://doi.org/10.1016/j.apsusc.2005.01.019.

(10) He, X.; Kwon, M.; Chung, J.; Lee, K.; Choi, Y.; Im, Y.; Jang, J.; Choi, Y.; Yoon, H. J. Self-Assembled Molecular Layers as Interfacial Engineering Nanomaterials in Rechargeable Battery Applications. *Small* **2024**, *20* (44), 2403537. https://doi.org/10.1002/smll.202403537.

(11) Yumnam, N.; Wagner, V. Controlled Growth of ZnO Nanorods via Self-Assembled Monolayer. *J Appl Electrochem* **2018**, *48* (1), 85–94. https://doi.org/10.1007/s10800-017-1134-6.
(12) Chaki, N. K.; Aslam, M.; Sharma, J.; Vijayamohanan, K. Applications of Self-Assembled Monolayers in Materials Chemistry. *J Chem Sci* **2001**, *113* (5), 659–670. https://doi.org/10.1007/BF02708798.
(13) Onclin, S.; Ravoo, B. J.; Reinhoudt, D. N. Engineering Silicon Oxide Surfaces Using Self-Assembled Monolayers. *Angewandte Chemie International Edition* **2005**, *44* (39), 6282–6304. https://doi.org/10.1002/anie.200500633.
(14) Vericat, C.; Vela, M. E.; Benitez, G.; Carro, P.; Salvarezza, R. C. Self-Assembled Monolayers of Thiols and Dithiols on Gold: New Challenges for a Well-Known System. *Chem. Soc. Rev.* **2010**, *39* (5), 1805–1834. https://doi.org/10.1039/B907301A.
(15) Adamkiewicz, M.; O'Hara, T.; O'Hagan, D.; Hähner, G. A Vapor Phase Deposition of Self-Assembled Monolayers: Vinyl-Terminated Films of Volatile Silanes on Silicon Oxide Substrates. *Thin Solid Films* **2012**, *520* (22), 6719–6723. https://doi.org/10.1016/j.tsf.2012.07.054.
(16) Adamkiewicz, M.; O'Hagan, D.; Haehner, G. Organic Chemistry on Surfaces: Direct Cyclopropanation by Dihalocarbene Addition to Vinyl Terminated Self-Assembled Monolayers (SAMs). *Beilstein J. Org. Chem.* **2014**, *10*, 2897–2902. https://doi.org/10.3762/bjoc.10.307.
(17) Wang, L.; Schubert, U.; Hoeppener, S. Surface Chemical Reactions on Self-Assembled Silane Based Monolayers. *Chemical Society Reviews* **2021**, *50*. https://doi.org/10.1039/D0CS01220C.
(18) Kolb, H. C.; Finn, M. G.; Sharpless, K. B. Click Chemistry: Diverse Chemical Function from a Few Good Reactions. *Angew Chem Int Ed Engl* **2001**, *40* (11), 2004–2021. https://doi.org/10.1002/1521-3773(20010601)40:11%253C2004::AID-ANIE2004%253E3.0.CO;2-5.
(19) Xi, W.; Scott, T. F.; Kloxin, C. J.; Bowman, C. N. Click Chemistry in Materials Science. *Advanced Functional Materials* **2014**, *24* (18), 2572–2590. https://doi.org/10.1002/adfm.201302847.
(20) Campos, M. A. C.; Paulusse, J. M. J.; Zuilhof, H. Functional Monolayers on Oxide-Free Silicon Surfaces via Thiol–Ene Click Chemistry. *Chem. Commun.* **2010**, *46* (30), 5512–5514. https://doi.org/10.1039/C0CC01264E.
(21) Llevot, A.; Steinmüller, S. O.; Bitterer, B.; Ridder, B.; Berson, J.; Walheim, S.; Schimmel, T.; Bräse, S.; Scheiba, F.; Meier, M. A. R. Sequence-Controlled Molecular Layers on Surfaces by Thiol–Ene Chemistry: Synthesis and Multitechnique Characterization. *Polym. Chem.* **2017**, *8* (38), 5824–5828. https://doi.org/10.1039/C7PY01515A.
(22) Yousaf, M. N.; Houseman, B. T.; Mrksich, M. Turning On Cell Migration with Electroactive Substrates. *Angewandte Chemie International Edition* **2001**, *40* (6), 1093–1096. https://doi.org/10.1002/1521-3773(20010316)40:6%253C1093::AID-ANIE10930%253E3.0.CO;2-Q.
(23) Ufheil, J.; Boldt, F. M.; Börsch, M.; Borgwarth, K.; Heinze, J. Microstructuring of Solid-Supported Lipid Layers Using SAM Pattern Generation by Scanning Electrochemical Microscopy and the Chemical Lens. *Bioelectrochemistry* **2000**, *52* (1), 103–110. https://doi.org/10.1016/S0302-4598(00)00090-8.

(24) Wendeln, C.; Ravoo, B. J. Surface Patterning by Microcontact Chemistry. *Langmuir* **2012**, *28* (13), 5527–5538. https://doi.org/10.1021/la204721x.
(25) Valles, D. J.; Naeem, Y.; Carbonell, C.; Wong, A. M.; Mootoo, D. R.; Braunschweig, A. B. Maskless Photochemical Printing of Multiplexed Glycan Microarrays for High-Throughput Binding Studies. *ACS Biomater. Sci. Eng.* **2019**, *5* (6), 3131–3138. https://doi.org/10.1021/acsbiomaterials.9b00033.
(26) Zhou, Y.; Xie, Z.; Brown, K. A.; Park, D. J.; Zhou, X.; Chen, P.-C.; Hirtz, M.; Lin, Q.-Y.; Dravid, V. P.; Schatz, G. C.; Zheng, Z.; Mirkin, C. A. Apertureless Cantilever-Free Pen Arrays for Scanning Photochemical Printing. *Small* **2015**, *11* (8), 913–918. https://doi.org/10.1002/smll.201402195.
(27) Carbonell, C.; Valles, D. J.; Wong, A. M.; Tsui, M. W.; Niang, M.; Braunschweig, A. B. Massively Multiplexed Tip-Based Photochemical Lithography under Continuous Capillary Flow. *Chem* **2018**, *4* (4), 857–867. https://doi.org/10.1016/j.chempr.2018.01.020.
(28) Li, J.; Li, L.; Du, X.; Feng, W.; Welle, A.; Trapp, O.; Grunze, M.; Hirtz, M.; Levkin, P. A. Reactive Superhydrophobic Surface and Its Photoinduced Disulfide-Ene and Thiol-Ene (Bio)Functionalization. *Nano Lett.* **2015**, *15* (1), 675–681. https://doi.org/10.1021/nl5041836.
(29) Dadfar, S. M. M.; Sekula-Neuner, S.; Trouillet, V.; Hirtz, M. A Comparative Study of Thiol-Terminated Surface Modification by Click Reactions: Thiol-Yne Coupling versus Thiol-Ene Michael Addition. *Advanced Materials Interfaces* **2018**, *5* (24), 1801343. https://doi.org/10.1002/admi.201801343.
(30) Le, C. M. Q.; Morlet-Savary, F.; Chemtob, A. Role of Thiol Oxidation by Air in the Mechanism of the Self-Initiated Thermal Thiol–Ene Polymerization. *Polym. Chem.* **2021**, *12* (45), 6594–6605. https://doi.org/10.1039/D1PY01301G.
(31) Le, N. H.; Bonne, M.; Airoudj, A.; Fioux, P.; Boubon, R.; Rebiscoul, D.; Bally-Le Gall, F.; Lebeau, B.; Roucoules, V. When Chemistry of the Substrate Drastically Controls Morphogenesis of Plasma Polymer Thin Films. *Plasma Processes and Polymers* **2021**, *18* (2), 2000183. https://doi.org/10.1002/ppap.202000183.
(32) Buffeteau, T.; Desbat, B.; Turlet, J. M. Polarization Modulation FT-IR Spectroscopy of Surfaces and Ultra-Thin Films: Experimental Procedure and Quantitative Analysis. *Appl Spectrosc* **1991**, *45* (3), 380–389. https://doi.org/10.1366/0003702914337308.
(33) Buffeteau, T.; Desbat, B.; Blaudez, D.; Turlet, J. M. Calibration Procedure to Derive IRRAS Spectra from PM-IRRAS Spectra. *Appl Spectrosc* **2000**, *54* (11), 1646–1650. https://doi.org/10.1366/0003702001948673.
(34) Ramin, M. A.; Le Bourdon, G.; Daugey, N.; Bennetau, B.; Vellutini, L.; Buffeteau, T. PM-IRRAS Investigation of Self-Assembled Monolayers Grafted onto SiO2/Au Substrates. *Langmuir* **2011**, *27* (10), 6076–6084. https://doi.org/10.1021/la2006293.
(35) Belman, N.; Jin, K.; Golan, Y.; Israelachvili, J. N.; Pesika, N. S. Origin of the Contact Angle Hysteresis of Water on Chemisorbed and Physisorbed Self-Assembled Monolayers. *Langmuir* **2012**, *28* (41), 14609–14617. https://doi.org/10.1021/la3026717.
(36) Wasserman, S. R.; Tao, Y. T.; Whitesides, G. M. Structure and Reactivity of Alkylsiloxane Monolayers Formed by Reaction of Alkyltrichlorosilanes on Silicon Substrates. *Langmuir* **1989**, *5* (4), 1074–1087. https://doi.org/10.1021/la00088a035.
(37) Snyder, R. G.; Strauss, H. L.; Elliger, C. A. Carbon-Hydrogen Stretching Modes and the Structure of n-Alkyl Chains. 1. Long, Disordered Chains. *J. Phys. Chem.* **1982**, *86* (26), 5145–5150. https://doi.org/10.1021/j100223a018.

(38) Wilbur, J. L.; Biebuyck, H. A.; MacDonald, J. C.; Whitesides, G. M. Scanning Force Microscopies Can Image Patterned Self-Assembled Monolayers. *Langmuir* **1995**, *11* (3), 825–831. https://doi.org/10.1021/la00003a025.
(39) Moores, B.; Simons, J.; Xu, S.; Leonenko, Z. AFM-Assisted Fabrication of Thiol SAM Pattern with Alternating Quantified Surface Potential. *Nanoscale Res Lett* **2011**, *6* (1), 185. https://doi.org/10.1186/1556-276X-6-185.
(40) Lü, J.; Delamarche, E.; Eng, L.; Bennewitz, R.; Meyer, E.; Güntherodt, H.-J. Kelvin Probe Force Microscopy on Surfaces: Investigation of the Surface Potential of Self-Assembled Monolayers on Gold. *Langmuir* **1999**, *15* (23), 8184–8188. https://doi.org/10.1021/la9904861.
(41) Hackl, T.; Schitter, G.; Mesquida, P. AC Kelvin Probe Force Microscopy Enables Charge Mapping in Water. *ACS Nano* **2022**, *16* (11), 17982–17990. https://doi.org/10.1021/acsnano.2c07121.
(42) Lee, S. H.; Ishizaki, T.; Saito, N.; Takai, O. Electrochemical Soft Lithography of an 1,7-Octadiene Monolayer Covalently Linked to Hydrogen-Terminated Silicon Using Scanning Probe Microscopy. *Surface Science* **2007**, *601* (18), 4206–4211. https://doi.org/10.1016/j.susc.2007.04.094.